

Sun-Pill Jung

Biorobotics Laboratory,
School of Mechanical and Aerospace Engineering/
SNU-IAMD,
Seoul National University,
1 Gwanak-ro, Gwanak-gu,
Seoul 151-742, Korea
e-mail: sunpill20@snu.ac.kr

Gwang-Pil Jung

Biorobotics Laboratory,
School of Mechanical and Aerospace Engineering/
SNU-IAMD,
Seoul National University,
1 Gwanak-ro, Gwanak-gu,
Seoul 151-742, Korea
e-mail: ceaser97@snu.ac.kr

Je-Sung Koh

Biorobotics Laboratory,
School of Mechanical and Aerospace Engineering/
SNU-IAMD,
Seoul National University,
1 Gwanak-ro, Gwanak-gu,
Seoul 151-742, Korea
e-mail: kjs15@snu.ac.kr

Dae-Young Lee

Biorobotics Laboratory,
School of Mechanical and Aerospace Engineering/
SNU-IAMD,
Seoul National University,
1 Gwanak-ro, Gwanak-gu,
Seoul 151-742, Korea
e-mail: winter2nf@gmail.com

Kyu-Jin Cho¹

Associate Professor
Biorobotics Laboratory,
School of Mechanical and Aerospace Engineering/
SNU-IAMD,
Seoul National University,
1 Gwanak-ro, Gwanak-gu,
Seoul 151-742, Korea
e-mail: kjcho@snu.ac.kr

Fabrication of Composite and Sheet Metal Laminated Bistable Jumping Mechanism

A layer-based manufacturing method using composite microstructures is widely used for mesoscale robot fabrication. This fabrication method has enabled the development of a lightweight and robust jumping robot, but there are limitations in relation to the embedding of elastic components. In this paper, a fabrication method for embedding an elastic component at an angled position is developed, extending the capability of the composite microstructures. This method is then used to build an axial spring attached to the bistable mechanism of a jumping robot. Sheet metal is used as an elastic component, which is stamped after the layering and curing process, thereby changing the neutral position of the spring. Two linear springs are designed to be in parallel with a joint to impose bistability; thereby delivering two stable states. This bistable mechanism is triggered with a shape memory alloy (SMA) coil spring actuator. A small-scale jumping mechanism is then fabricated using this mechanism; it jumps when the snap-through of the bistable mechanism occurs. A model of the stamped sheet metal spring is built based on a pseudo rigid body model (PRBM) to estimate the spring performance, and a predictive sheet metal bending model is also built to design the die for stamping. The experimental results show that the stamped sheet metal spring stores 12.63 mJ of elastic energy, and that the mechanism can jump to a height of 175 mm with an initial takeoff velocity of 1.93 m/s. [DOI: 10.1115/1.4029489]

Introduction

Jumping is an effective method used by small-scale robots to overcome obstacles larger than their size. Most jumping robots use catapult mechanisms to obtain sufficient momentum with limited actuator power. The various parts of a jumping robot, which use the catapult mechanism, i.e., the legs, body, energy storage spring, transmission, and actuator, are fabricated separately or purchased “off the shelf” and used to assemble the robot [1–7]. However, these parts are extremely small and therefore the self-assembly of a jumping robot is not very practical.

Small-scale jumping robots that use a simple integrative fabrication process, i.e., a microelectromechanical systems (MEMS) process or a smart composite microstructure (SCM) has been developed. Bergbreiter developed a jumping microrobot with polydimethylsiloxane (PDMS) as the elastic component [8]. For jumping, Chevron actuators are used to linearly pull and release

the PDMS spring that is embedded into an etched silicon dioxide structure. A flea-inspired jumping robot that uses a torque reversal mechanism has also been developed using an SCM based process [9,10]. The moving components are laminated into one piece with a composite of glass fiber and polyimide (PI) while the energy storage elements and actuators (the SMA coil springs) are attached by manual soldering. In addition, a simplified torque reversal mechanism has been developed that reduced the number of required actuators [11]. Beam patterned composite is used as a bending spring for passive triggering and energy storage, and a single SMA coil spring actuator is used to bend the beam patterned composite, which reverses the torque and creates the momentum for jumping.

However, the current integrative mode of fabrication has limitations in relation to embedding various types of elastic components (such as axial springs and rotational springs) at a desired position and angle. Unlike body parts that can be designed in 2D and then folded to a 3D shape [12,13], springs designed in 2D cannot be simply folded into a 3D shape; in a patterned beam spring, the neutral position of a spring will always be flat.

To embed the elastic components for various mechanisms, it is necessary to control the spring's neutral position, and two

¹Corresponding author.

Manuscript received August 19, 2014; final manuscript received December 23, 2014; published online February 27, 2015. Assoc. Editor: Aaron M. Dollar.

methods can be used for controlling the neutral position. The first method uses a laminated elastic sheet component that is preloaded. Because it is preloaded, the laminated structure with moving joints naturally rotates to a stable position. The other method uses memorizing of the neutral position after the curing process. The former method requires a stretchable sheet material that can be laminated in a stretched state. However, embedding a stretched sheet can induce misalignment or a delamination problem during lamination. If the neutral position can be changed after the curing process, problems related to the preload can then be solved. Therefore, the latter is suitable for SCM. This method requires some sheet materials that can sustain the deformed shape, such as the sheet metal.

In this paper, a fabrication method for embedding an elastic component at an angled position is developed, extending the capability of the composite microstructures. This method is then used to build a linear spring attached to the bistable mechanism of a jumping mechanism. Sheet metal is used as an elastic component, and this is stamped after the layering and the curing process, thereby changing the neutral position of the spring. Extra joints at both ends of the stamped sheet spring enable it to function as an axial spring. Two axial springs are designed to be in parallel to a joint, which imposes bistability, thereby enabling two stable states. These springs store a large amount of energy, which is released when triggered with a SMA coil spring actuator. A small-scale jumping mechanism is then fabricated using this mechanism, which jumps when the snap-through of the bistable mechanism occurs. A model of the stamped sheet metal spring is built based on a PRBM and used to estimate the spring performance. In addition, a predictive sheet metal bending model is also built to find design of the die for stamping. The experimental results show that the stamped sheet metal spring stores 12.63 mJ

of elastic energy and the mechanism can jump to a height of 175 mm with a takeoff velocity of 1.93 m/s.

Conceptual Design

Elastic components are essential in a jumping mechanism as they store the elastic energy used to jump. Energy generated by an actuator is gradually stored as elastic energy in a spring, which when triggered instantly releases the stored energy and enables jumping. This section presents a design concept that uses a bistable mechanism for jumping and includes a new fabrication method for embedding a spring into the bistable mechanism.

Design of the Bistable Jumping Mechanism. The bistable structure is shown in Fig. 1(a). It consists of two rigid links and one axial spring. The two rigid links are connected to each other by a rotational joint, and the axial spring is connected between the rigid links. By unfolding the rigid links, the axial spring is stretched, thereby increasing the total structural energy. The links are rotated until the axial spring passes through the rotational joint, and at this point, the direction of the moment induced from the axial spring changes rapidly, causing snap-through. With respect to energy, this means that the structural energy of this state overcomes the threshold energy. After passing this snap-through point, the rigid links fold and the elastic energy is released until the mechanism reaches another stable shape (Fig. 1(b)).

The actuating method of this bistable structure is shown in Fig. 2. Two additional triggering beams are connected to the ends of the bistable structure with rotational springs, and SMA coil spring actuators are attached to each tip of the triggering beam, as shown in Fig. 2(a). The SMA coil spring shrinks, and the triggering beams then start to rotate (as shown in Fig. 2(b)). Continuous

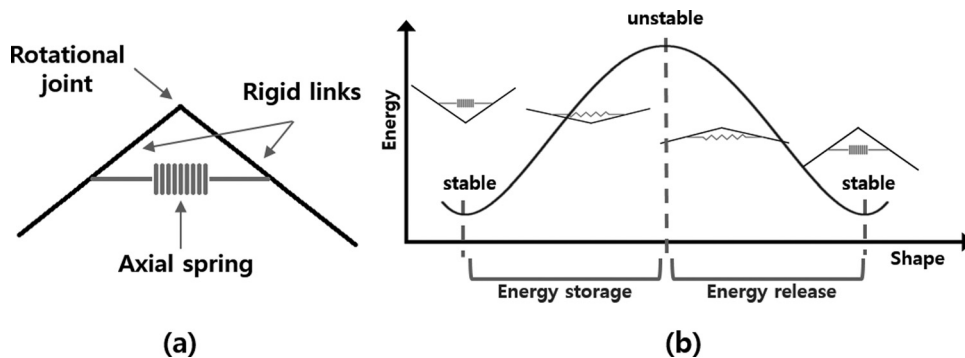


Fig. 1 (a) Simple bistable structure. (b) Conceptual graph of elastic energy in relation to the shape of the bistable structure.

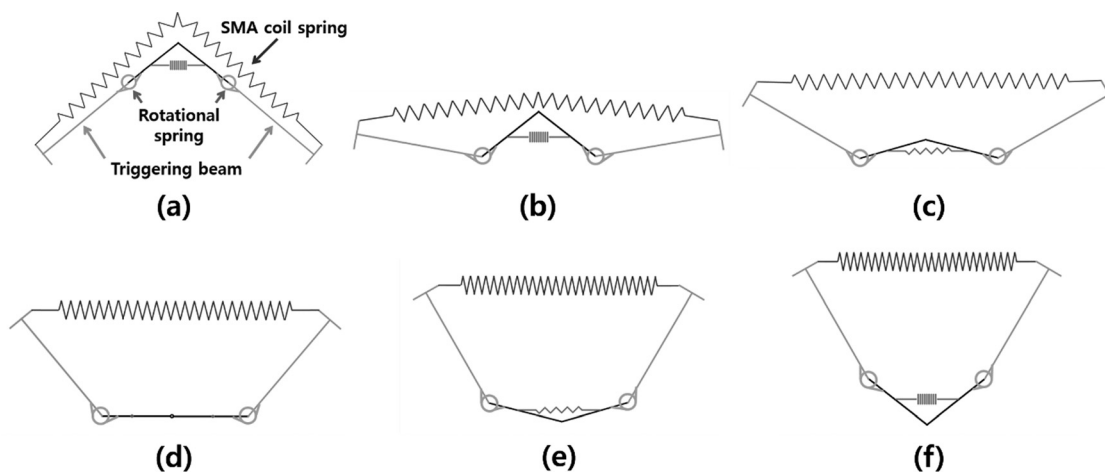


Fig. 2 Conceptual design of the bistable jumping mechanism and schematic drawing of bistable structure actuation

rotation of the triggering beams increases the length of the moment arm (Fig. 2(c)). The bistable structure then starts to unfold, thereby storing the elastic energy in the axial spring, and the SMA coil spring shrinks until the axial spring passes the snap-through point (Fig. 2(d)). After passing the snap-through point, the direction of the moment induced by the axial spring changes (Fig. 2(e)). In this phase, the elastic energy stored in the elastic components (two rotational springs and the axial spring) releases simultaneously, causing the mechanism to jump. The energy releasing process continues until the structure becomes stable (Fig. 2(f)).

Energy stored in the bistable mechanism is determined by the sum of elastic energy stored in the two rotational springs and one axial spring. The structural energy in the bistable structure is determined by the threshold energy. The threshold energy is determined by the axial spring. As the stiffness of the axial spring increases, the energy to achieve snap-through also increases, which increases the total stored energy in the bistable structure.

Stamped Sheet Metal Spring Used in Composite Laminated Fabrication. This section presents the integrative structure of the spring component using a stamped sheet metal spring. SCM processes [14] have generally been used in small-scale structures [15–19]. Glass or carbon fiber composites are patterned as the rigid links, and the PI film acts as a rotational joint. However, the current SCM process is limited in relation to embedding useful elastic components, and currently only a patterned composite beam bending spring exists. Therefore, the problem is that the neutral position of the spring lies in a flat position, which limits the design as various mechanisms require the spring's neutral position to be at an angled position. To solve this problem, we developed a method of changing the neutral position by stamping, which plastically deforms the sheet metal (the fabricated structure

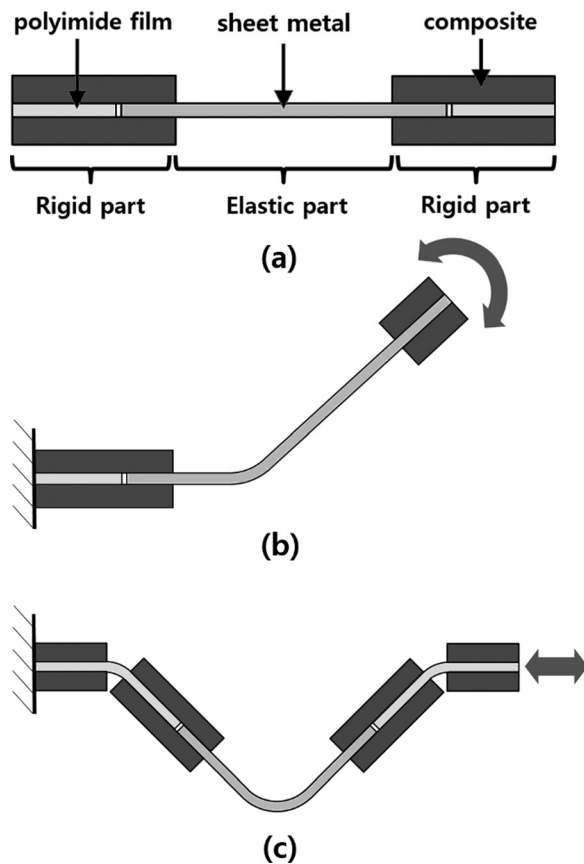


Fig. 3 (a) SCM process with sheet metal, (b) rotational spring with stamped sheet metal, and (c) axial spring with stamped sheet metal

is schematically shown in Fig. 3(a)). The sheet metal partly replaces the PI film, which is normally used as joints, and takes the role of both rotational spring and axial spring, according to the arrangement and post stamping process. The sheet metal acting as rotational spring is shown in Fig. 3(b). It can be made by replacing the PI joint and stamping the sheet metal to attain the desired neutral position. The stiffness of the rotational spring is determined by the shape parameters and material properties of the stamped sheet metal.

As shown in Fig. 3(c), the structure acting as an axial spring has three joints. One metal sheet is situated in the middle of the structure and two freely rotating PI film joints are located on both sides. To obtain axial elasticity, the sheet metal is bent by stamping to attain a shrunken neutral position. This stamped sheet metal can then move (in the direction of the arrow indicated in Fig. 3(c)), allowing the PI joints to freely rotate. Stiffness of the axial spring is determined by the shape parameters and material properties of the sheet metal.

The bistable jumping mechanism consists of a body with one axial spring, two rotational springs on both sides, and one SMA coil spring actuator for the trigger, as shown in Fig. 4. The mechanism is the same as that described in Fig. 2.

Simplified Spring Stiffness Design for Stamped Sheet Metal

The stamped sheet metal spring for an axial spring is the key component for the bistable jumping mechanism since the axial spring determines the threshold energy and the total structural energy. To design the stamped sheet metal spring having desired threshold energy, following spring geometric dimensions are considered: L is the total length of the unstamped sheet metal spring, L_c is the length of the structure clamping the metal sheet, $D_{neutral}$ is the length of the stamped sheet metal spring's neutral position, D_{max} is the maximum deflected length of the spring, and E_{stored} is the stored elastic energy at D_{max} .

$D_{neutral}$, D_{max} , L , and L_c are shown in Fig. 5 and determined at the beginning of the design process for the jumping mechanism. To predict E_{stored} in the desired mechanism design, it is necessary

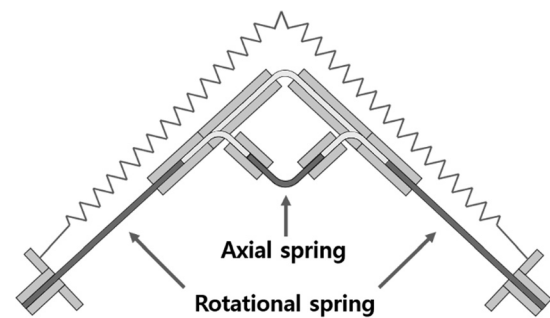


Fig. 4 Implementation of the conceptual bistable jumping mechanism using stamped sheet metal

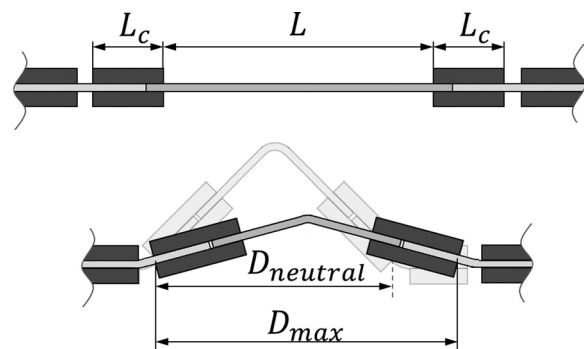


Fig. 5 Parameters of the sheet metal spring

to model the stamped sheet metal. In general, large deflection analysis based on solid mechanics delivers reasonably quite accurate results; however, it requires high computational costs. In this study, the PRBM is adopted as a modeling method, as this delivers a simple and efficient prediction of the sheet metal spring model [20].

Modeling of Stamped Sheet Metal. The model is divided into three regions: two cantilever beams (l_2) and one curved beam ($2l_1$) which consist of rigid links and torsional springs (as shown in Fig. 6). Force and moment are applied at the end of each beam. As the applied moment in a beam creates a curvature in the beam, each beam can be represented by an initially curved beam with a force [20].

Figure 7 shows the PRBM of the end moment loading. The modeling parameters are the characteristic radius factor (γ) and the parametric angle coefficient of the moment loading ($c_{\theta,m}$). According to the shape of the beam, the values of γ and $c_{\theta,m}$ varies. However, they hardly vary over a large range of the curved beam's shape. Therefore, the values of γ and $c_{\theta,m}$ can be approximated to the constant average value ($\gamma \approx 0.83$, $c_{\theta,m} \approx 1.64$) [20], and the torsional spring constant K_{moment} is approximately calculated using the following equation:

$$\begin{cases} K_{\text{moment}} = c_{\theta,m} \frac{EI}{l} \approx 1.64 \frac{EI}{l} \\ \theta_i = a \tan\left(\frac{b_i}{a_i - l(1-\gamma)}\right) \approx a \tan\left(\frac{b_i}{a_i - 0.17l}\right) \\ \phi_m = c_{\theta,m}(\Theta_i + \theta_m) \approx 1.64(\Theta_i + \theta_m) \end{cases} \quad (1)$$

Figure 8 shows the PRBM of the force loading on the curved beam by the moment. The additional modeling parameters are the parametric angle coefficient for force loading ($c_{\theta,f}$) and the stiffness coefficient (K_{θ}). Although the value of $c_{\theta,f}$ varies according

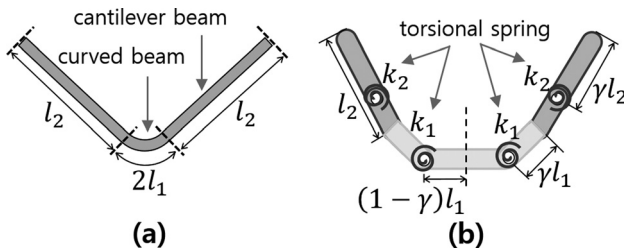


Fig. 6 (a) Model of stamped sheet metal. (b) Simplified model including rigid links and torsional springs.

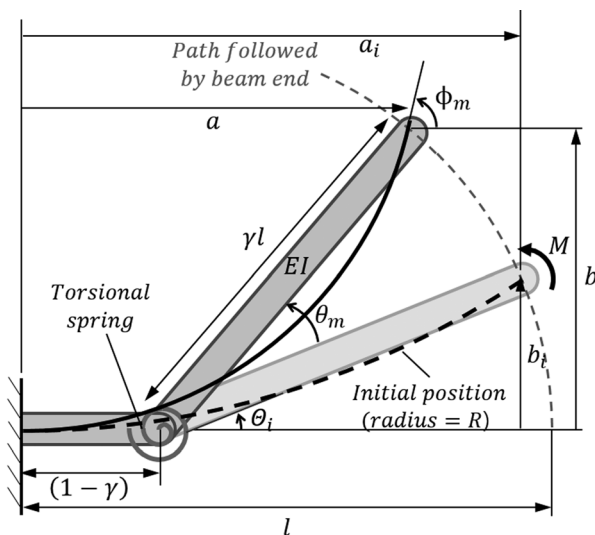


Fig. 7 PRBM of the end moment loading

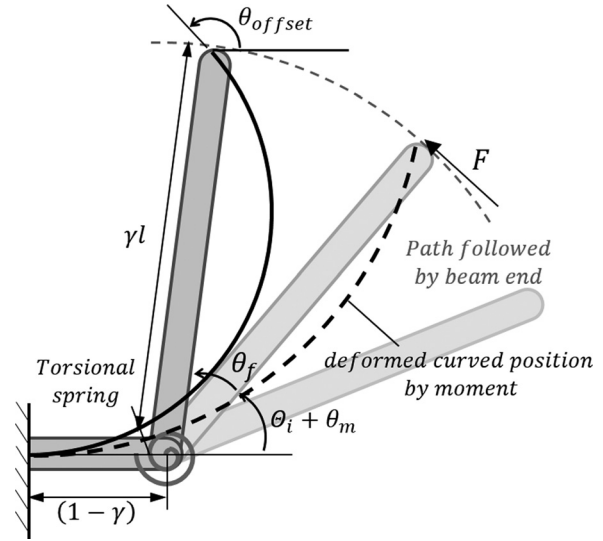


Fig. 8 Pseudo rigid model of the force loading on the curved beam by the moment

to the direction of the force applied to the beam, it hardly varies over a large range of force angle. Similar to the case of moment loading, the value of $c_{\theta,f}$ can be approximated to the constant average value ($c_{\theta,f} \approx 1.228$), and K_{θ} can be approximated to $\pi\gamma$ (≈ 2.67) [20]. Then, the beam tip's direction (θ_{offset}) and the torsional spring constant K_{force} is therefore approximately calculated using the following equation:

$$\begin{cases} K_{\text{force}} = \gamma K_{\theta} \frac{EI}{l} \approx 2.16 \frac{EI}{l} \\ \theta_{\text{offset}} = c_{\theta,f} \theta_f + \phi_m = c_{\theta,f} \theta_f + c_{\theta,m}(\Theta_i + \theta_m) \end{cases} \quad (2)$$

As shown in Fig. 9, the half side of the axial spring in the bistable jumping mechanism can be simplified with two torsional springs and links by utilizing Eqs. (1) and (2). The variables θ_1 and θ_2 are

$$\begin{cases} \theta_1 = \theta_{1,m} + \theta_{1,f} \\ \theta_2 = \theta_{2,m} + \theta_{2,f} \end{cases} \quad (3)$$

where $\theta_{i,m}$ is deformed angle by moment loading, and $\theta_{i,f}$ is deformed angle by force loading in the i th beam. The moment equilibrium equations induced by the moment and the force can be represented as follows:

$$\begin{cases} F \times (\gamma l_1 \sin(\Theta_{1,i} - \theta_1)) = \gamma K_{\theta} \frac{EI}{l_1} \times \theta_{1,f} \\ M_1 = F h_1 = c_{\theta,m} \frac{EI}{l_1} \times \theta_{1,m} \\ h_1 = ((1-\gamma)l_2 \sin(\theta_{1,\text{offset}}) + \gamma l_2 \sin(\theta_{1,\text{offset}} - \theta_2) + L_c \sin(\theta_{1,\text{offset}} - \theta_{2,\text{offset}})) \end{cases} \quad (4)$$

$$\begin{cases} F \times (\gamma l_2 \sin(\theta_{1,\text{offset}} - \theta_2)) = \gamma K_{\theta} \frac{EI}{l_2} \times \theta_{2,f} \\ M_2 = F h_2 = c_{\theta,m} \frac{EI}{l_2} \times \theta_{2,m} \\ h_2 = L_c \sin(\theta_{1,\text{offset}} - \theta_{2,\text{offset}}) \end{cases} \quad (5)$$

These equations are solved using MATLAB, and $\theta_{1,m}$, $\theta_{1,f}$, $\theta_{2,m}$, and $\theta_{2,f}$ are determined according to the applied force. The displacement is given as

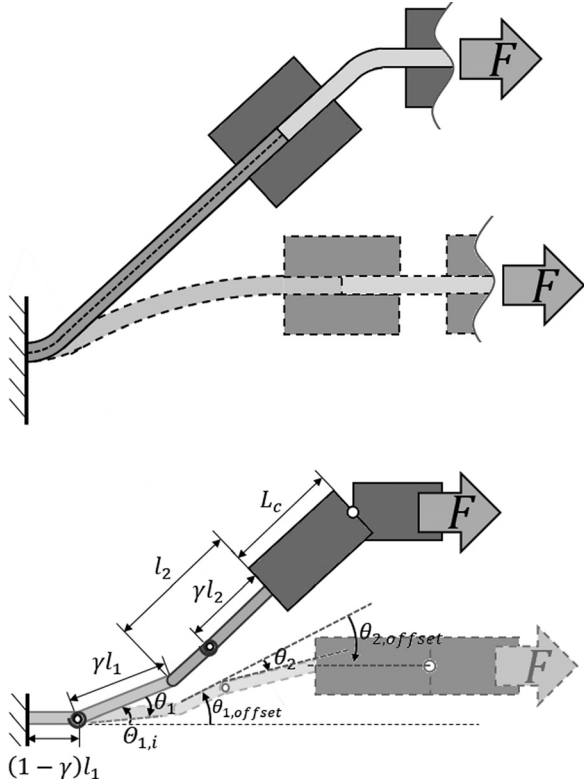


Fig. 9 Simplified model of the half side of an axial spring in the bistable jumping mechanism

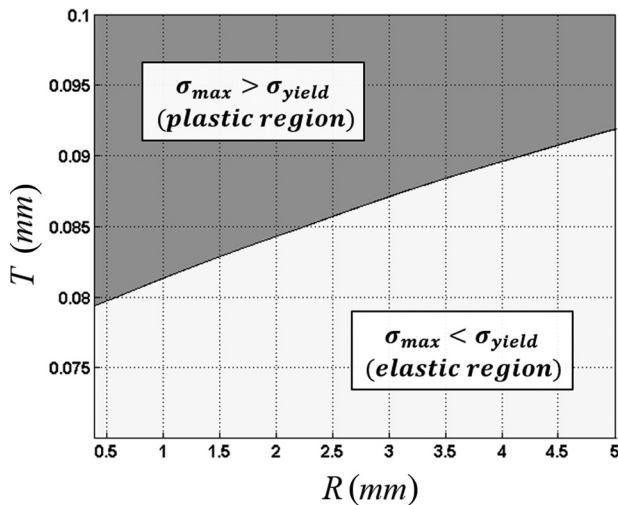


Fig. 10 Graphical representation of the combination of R and T in elastic region ($w = 5 \text{ mm}$, $D_{\text{neutral}} = 25.6 \text{ mm}$, $D_{\text{max}} = 30.8 \text{ mm}$, $L = 22 \text{ mm}$, $L_c = 9.5 \text{ mm}$)

$$D = 2\{(1 - \gamma)l_1 + \gamma l_1 \cos(\Theta_{1,i} - \theta_1) + (1 - \gamma)l_2 \cos(\theta_{1,\text{offset}}) + \gamma l_2 \cos(\theta_{1,\text{offset}} - \theta_2) + L_c \sin(\theta_{1,\text{offset}} - \theta_{2,\text{offset}})\} \quad (6)$$

Stamped Sheet Metal Design. When designing the stamped sheet metal, deflection of the sheet metal needs to be limited in the elastic range ($\sigma_{\text{max}} < \sigma_{\text{yield}}$). We consider two parameters for designing available stamped sheet metal springs: T being the thickness of sheet metal, and R being the stamped radius of sheet metal.

The maximum stress (σ_{max}) is defined as Ref. [19]

$$\sigma_{\text{max}} = \frac{M_1 y}{I} + \frac{F(\rho l_1 \sin(\Theta_{1,i} - \theta_1))y}{I} + \frac{F}{A} \quad (7)$$

where y is the distance from the neutral line to the outer surface of the beam. To simplify the analysis, the neutral line is set as the middle line of the beam. The elastic region is therefore represented as follows:

$$\sigma_{\text{max}} = F \left(\frac{T}{2I} (h_1 + \rho l_1 \sin(\Theta_{1,i} - \theta_1)) + \frac{1}{A} \right) < \sigma_{\text{yield}} \quad (8)$$

Available combinations of R and T for the designed mechanism can be obtained by using Eq. (8). Figure 10 shows the available combination of R and T . In addition, to evaluate effect of R and T to the stored elastic energy (E_{stored}), the force–displacement relationship of the stamped sheet metal spring model is presented in Fig. 11. In Fig. 11(a), the stiffness of the sheet metal spring did not change much with the change of the radius. On the other hand, as the thickness increased, the stiffness of sheet metal spring and the stored energy largely increased in Fig. 11(b).

Predictive Sheet Metal Bending Model

The bistable jumping mechanism is fabricated using the integrative SCM process and a layer of sheet metal as shown in Fig. 12. After the curing process, the sheet of metal is bent using the stamping method to alter the neutral position. However, making the desired shape of sheet metal spring by stamping is not easy because of the “springback” phenomenon. It causes a difference between the stamped shape of the sheet metal and the shape of the stamping die. To determine the required shape of the die that will deliver the sheet metal’s desired state, a predictive sheet metal model is developed in this section.

One of the most common bending methods used to bend a piece of a sheet metal is wiping die bending, also known as edge bending (Fig. 13). The shape parameters are the edge radius of the die and its angle. The pad and die hold the sheet metal and the flange then slides down along the pad and pushes the sheet metal (which protrudes from the pad and the die). Although the released sheet metal is bent after unloading, it does not have the same shape of the die because of the springback phenomenon [22].

A schematic diagram of the springback phenomenon is shown in Fig. 14. The springback parameters are: T , the thickness of the sheet metal; R_i , the initial loading bending radius (edge radius of die); θ_{initial} , the initial loading bending angle (edge angle of die); R_f , the final bended inner radius of the sheet metal after being unloaded; R , the final bended neutral radius of the sheet metal ($R = R_f + T/2$); and θ_{final} , the final bended angle of the sheet metal after being unloaded.

Elastic recovery changes the initial parameters to the final parameters after stamping; R_f is larger than R_i , and θ_{final} is smaller than θ_{initial} . To obtain the desired final shape of the sheet from the initial die’s shape parameters, it is thus necessary to develop a predictive model of the amount of springback that will occur. Since the length of the neutral lines is constant, we get

$$L_n = \left(R_i + \frac{T}{2} \right) \theta_{\text{initial}} = \left(R_f + \frac{T}{2} \right) \theta_{\text{final}} \quad (9)$$

$$K_s = \frac{R_i + \frac{T}{2}}{R} = \frac{\theta_{\text{final}}}{\theta_{\text{initial}}} \quad (10)$$

The springback factor (K_s) is a material property known to be the function of R_i/T [22]. The springback factors are obtained by switching the dies having various shape parameters by experiments as shown in Fig. 15.

To obtain the desired shape of the sheet metal, the die’s shape parameters (R_i and θ_{initial}) can be determined as follows:

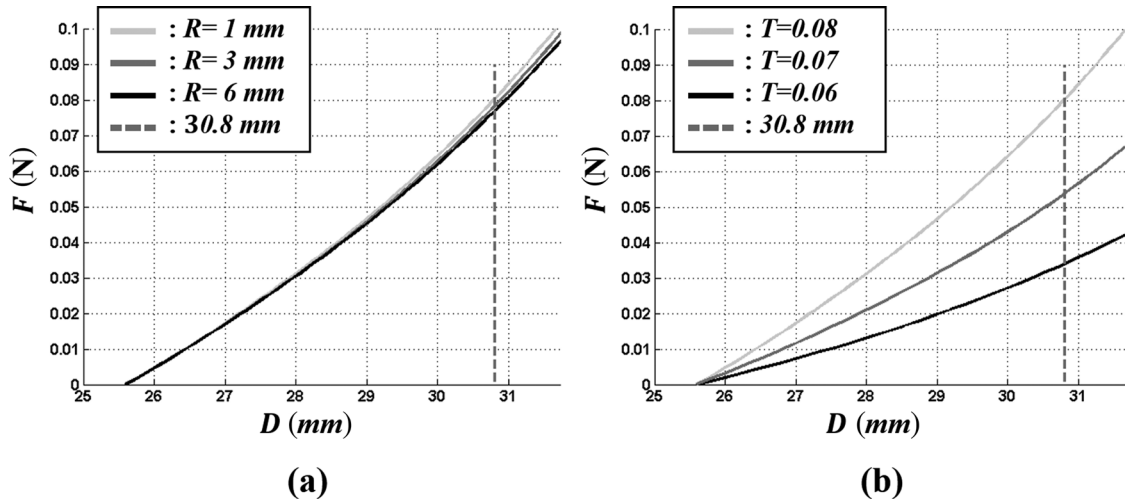


Fig. 11 The force-deflection relationship of the stamped sheet metal spring model ($w = 5$ mm, $D_{\text{neutral}} = 25.6$ mm, $D_{\text{max}} = 30.8$ mm, $L = 22$ mm, $L_c = 9.5$ mm); (a) when R varies with constant T ($= 0.08$ mm) and (b) when T varies with constant R ($= 1$ mm)

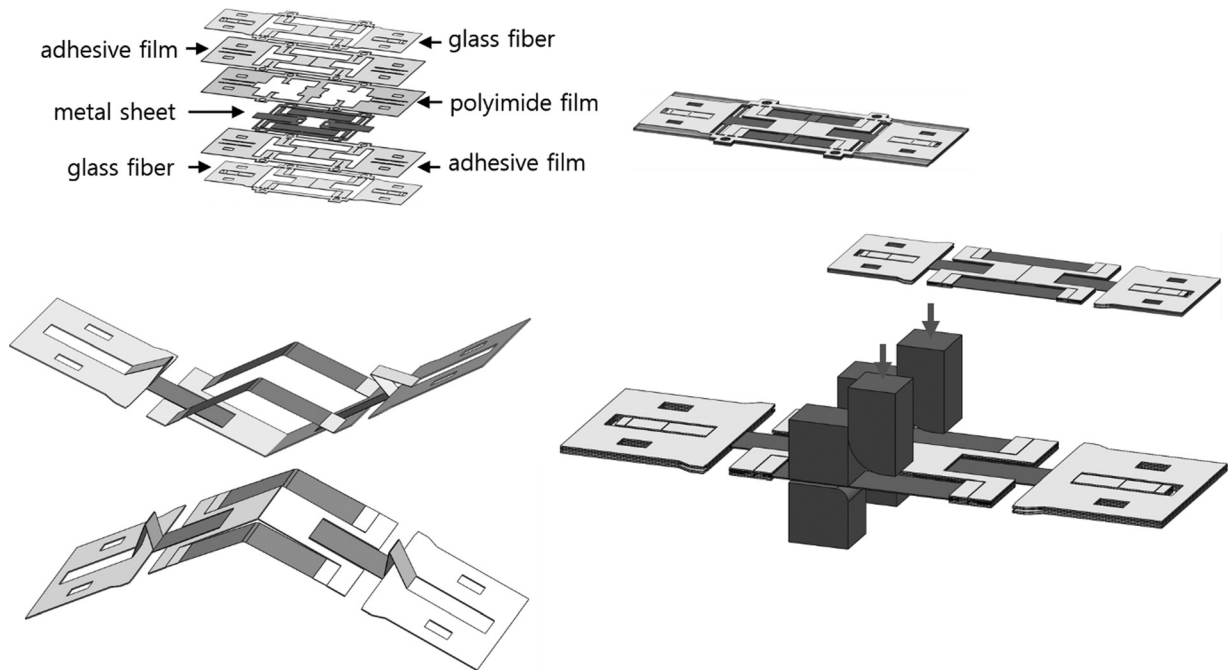


Fig. 12 Fabrication process of bistable jumping mechanism with the spring integrative SCM process using stamping the sheet metal

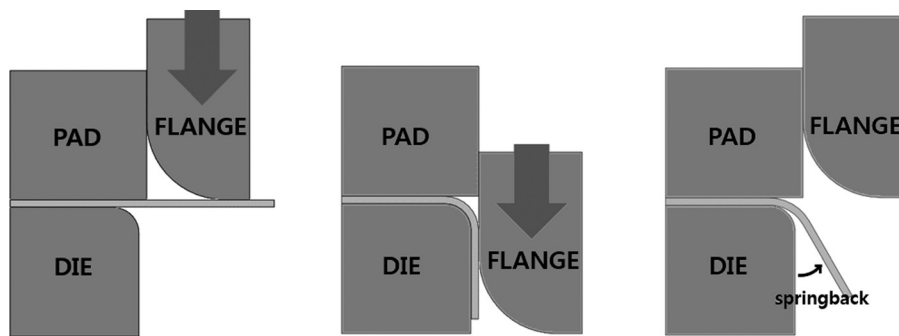


Fig. 13 Wiping die bending method

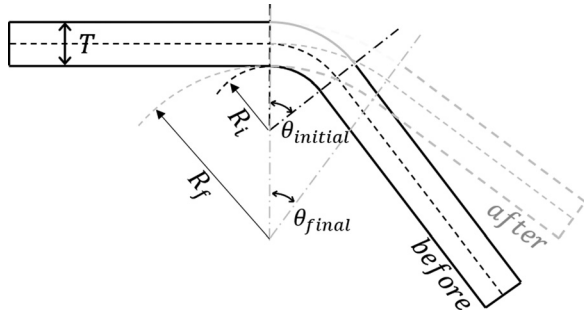


Fig. 14 Schematic diagram of springback phenomenon

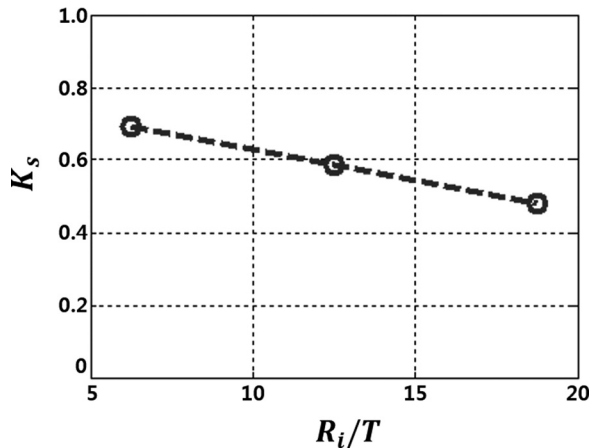


Fig. 15 Experimental results of the springback factor versus R_i/T

known $R_{\text{final}}, \theta_{\text{final}} \rightarrow$ find $R_i, \theta_{\text{initial}}$

Let $x = \frac{R_i}{T}$, $A = \frac{R_f}{T} + \frac{1}{2} = \frac{R}{T}$

$$K_s(x) = \frac{x + \frac{1}{2}}{A} \Leftrightarrow \frac{R}{T} K_s(x) - x - \frac{1}{2} \approx \frac{R}{T} (-0.0169x + 0.37981) - x - \frac{1}{2} = 0 \quad (11)$$

x can be found

$$\therefore R_i = xT, \quad \theta_{\text{initial}} = \left(\frac{1}{K_s(x)} \right) \theta_{\text{final}} \quad (12)$$

Meanwhile, D_{neutral} gives the value of θ_{final} ($D_{\text{neutral}} = 2(R_{\text{sin}}(\theta_{\text{final}}/2) + ((L - R\theta_{\text{final}})/2 + L_c)\cos(\theta_{\text{final}}/2))$, and the maximum bending angle, θ_{initial} , is limited to 180deg in current stamping method. The boundary condition is therefore obtained as following equation:

$$\left(\frac{1}{K_s(x)} \right) \theta_{\text{final}} = \theta_{\text{initial}} \leq \pi \Leftrightarrow \theta_{\text{final}} \leq \pi K_s(x) \approx \frac{\pi}{2} (-0.0169x + 0.7981) \quad (13)$$

By using Eqs. (11) and (13), the available value of R , T , and D_{neutral} can be determined.

Results

Experiments and simulations are conducted to verify the predictive sheet metal bending model and the simplified stamped sheet metal spring model. In addition, the fabrication result is presented and a jumping test is performed to demonstrate the capabilities of the bistable jumping mechanism.

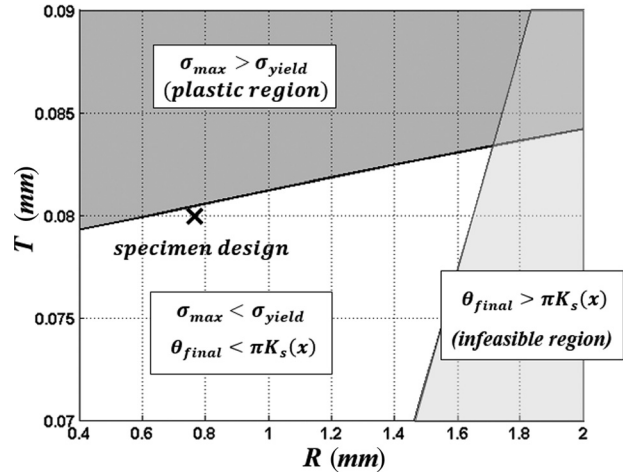


Fig. 16 Graphical representation of the available combination of R and T and the position of the specimen ($w = 5$ mm, $D_{\text{neutral}} = 25.6$ mm, $D_{\text{max}} = 30.8$ mm, $L = 22$ mm, $L_c = 9.5$ mm)

Comparison Between Sheet Metal Spring Model and Experimental Result. The neutral position of the stamped metal sheet spring (SUS 304) was designed as 25.6 mm and the maximum deflection was 30.8 mm. In addition, the length of the specimen was 41 mm ($L = 22$ mm and $L_c = 9.5$ mm), and the width (w) was 5 mm. The available combination of R and T was obtained as shown in Fig. 10. In addition, the designed specimen should be in the available region determined by Eq. (13). Finally, R and T were determined as $R = 0.74$ mm and $T = 0.08$ mm as shown in Fig. 16.

To obtain the designed sheet metal spring specimen, the die's shape parameters were determined by Eq. (12), and then R_i and θ_{initial} were calculated as 0.5 mm and 2.618 rad. The specimen was stamped by wiping bending die, and then the bent specimen achieved parameters of $R = 0.74$ mm and $\theta_{\text{final}} = 1.752$. The achieved specimen's neutral position had slight difference compared to the designed specimen's neutral position with an error of 3.5%.

Figure 17 shows the force–displacement relationship of the spring model and the experimental results. The experiment was conducted by changing the displacement and measuring the force. As shown in Fig. 17, the model tends to follow the experimental results. Stored energy of the model and the fabricated specimen were 0.133 mJ and 0.119 mJ, respectively. The amount of difference in stored energy was 0.014 mJ. Geometric dimensions and parameters of the specimen are given in Table 1.

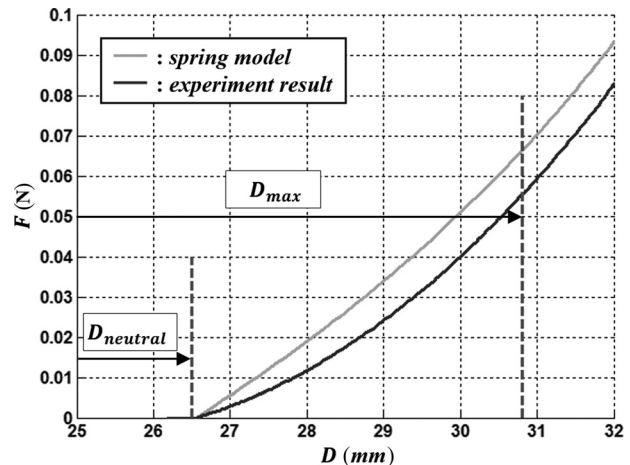


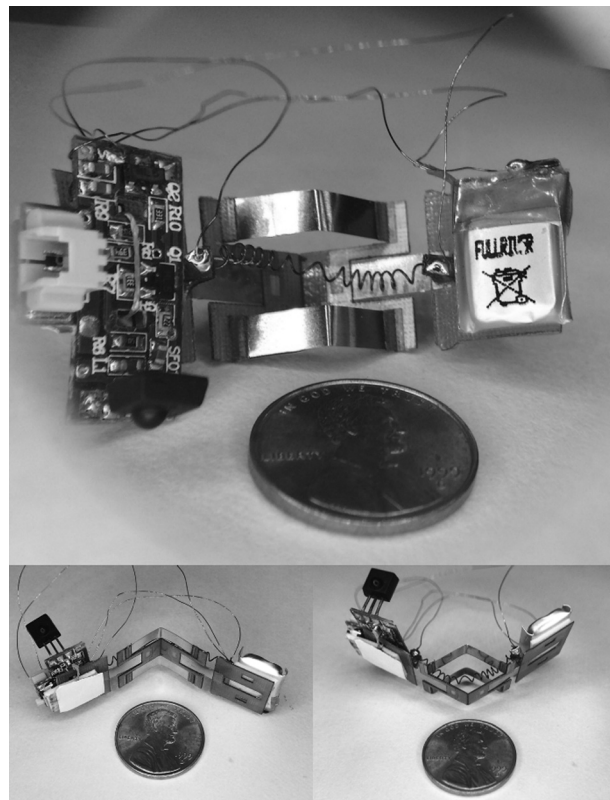
Fig. 17 Comparison between simplified force–deflection model and experimental results

Table 1 Specification of the specimen

Geometric dimensions	
$D_{neutral}$	26.5 mm
D_{max}	30.8 mm
ΔD_{max}	4.3 mm
L	22 mm
L_c	9.5 mm
w	5 mm
Parameters	
T	0.08 mm
R	0.74 mm
θ_{final}	1.752
$E_{elastic}$	
0.133 mJ (Spring model)	0.119 mJ (Experimental)

Fabrication Results. The bistable jumping mechanism was fabricated using laser machining, laminating, curing, and stamping. The glass fiber composites, PI film, and the sheet metal were patterned to act as the rigid links, the rotational joints, and elastic components, respectively. In the mechanism structure design process, sheet metal spring's geometric dimensions are considered as: $D_{neutral} = 15.7$ mm, $D_{max} = 17.2$ mm, $L = 15$ mm, and $L_c = 1.5$ mm.

Sheet metal with a thickness of 0.08 mm was used as the axial spring component and was stamped to achieve a radius of 2.6 mm and an angle (θ_{final}) of 1.082. For triggering beam, sheet metal with a thickness of 0.1 mm was used as the rotational spring component. After fabricating the integrative mechanism's structure, an IR receiver module and battery were added for wireless control as shown in Fig. 18. The prototype has two stable shapes and a

**Fig. 18 Fabrication results of the bistable jumping mechanism**

mass of 2.32 g (a main frame mass of 0.43 g and electrical device mass of about 1.9 g). When unfolded, the main body has a width of 51 mm width and a length of 22 mm. The spring integrative body frame has a mass of 0.43 g, width of 51 mm, and length of 16 mm without the electronics.

The SMA coil spring (Dynalloy Co., Irvine, CA) was clamped onto the glass fiber composite body as an actuator [23]. The SMA coil spring was designed based on the conventional spring equation ($F = (Gd^4/8D^3N)\delta$) and has the stiffness of 110.9 N/m in austenite phase. Specifications of the bistable jumping mechanism and dimensions of the SMA coil spring are given in Table 2.

Jumping Performance. The SMA coil spring has 1.5 Ω of electric resistance, and 0.67 A flows through the SMA coil spring for 3.6 s (2400 mJ). The bistable jumping mechanism took off within 2 ms as shown in Fig. 19, with a velocity of 1.93 m/s. Kinetic energy was computed as 4.34 mJ. Theoretically, the jumping height of the mechanism was 191 mm without consideration of air drag. However, in the experiments, the jumping height was shown to be actually 175 mm due to air drag, as shown in Fig. 20.

Energy induced from the SMA coil spring is stored in the sheet metal as elastic energy. After snap-through, the elastic energy is converted into kinetic energy, and finally kinetic energy is converted into potential energy. To evaluate the conversion efficiency showing the ratio of kinetic energy to initially stored energy, the amount of energy in each step was computed.

The SMA coil spring originally shrinks from 25.6 mm to 5.2 mm (23.05 mJ) when actuated. However, the mechanism cannot fully use the stored energy in the actuator since the SMA coil spring still shrinks while the mechanism takes off. At the instance of take-off, the length of SMA coil spring is 18.32 mm. This means that only 13.51 mJ is transferred to the mechanism from the SMA coil spring.

The elastic energy stored in the sheet metal springs was calculated by using simplified spring model. The unstamped rotational

Table 2 Specifications of the bistable jumping mechanism

Axial sheet metal spring (stamped component)	
$D_{neutral}$	15.7 mm
D_{max}	17.2 mm
ΔD_{max}	1.5 mm
L	15 mm
L_c	1.5 mm
w	4 mm
T	0.08 mm
R	2.6 mm
$E_{elastic}$	0.79 mJ
Rotational sheet metal spring (unstamped component)	
$D_{neutral}$	8 mm
L	8 mm
w	4 mm
T	0.1 mm
Mechanism body frame (with electrical device)	
Width	51 mm
Length	16 mm (22 mm with electronics)
Weight	0.43 g (2.32 g with electronics)
SMA coil spring actuator	
Wire diameter (d)	250 μ m
Coil diameter (D)	1.76 mm
Coil number (N)	13.5
Theoretical spring constant (k) (actuation)	121.11 N/m
Measured spring constant (k) (actuation)	110.9 N/m
Initial length	25.6 mm
Final length	5.2 mm

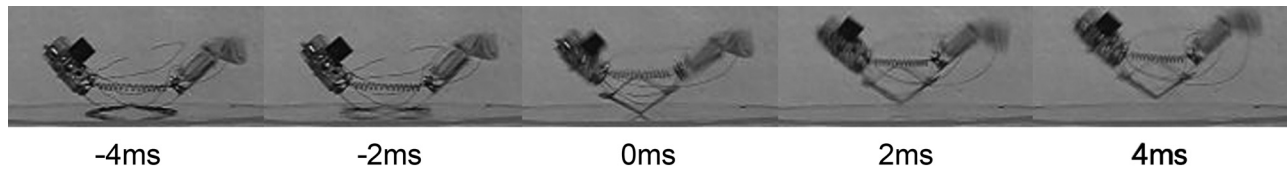


Fig. 19 Sequential high-speed images of bistable jumping mechanism at takeoff

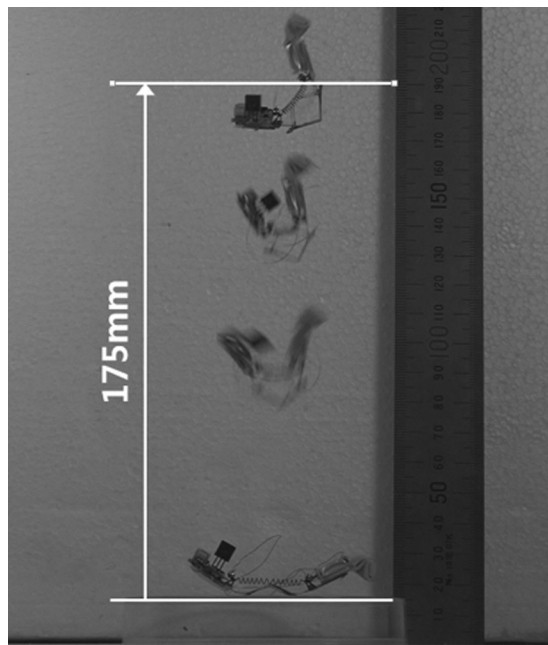


Fig. 20 Jumping trajectory of bistable jumping mechanism

Table 3 Energy and conversion rate in the bistable jumping mechanism

	Energy (mechanical)	Conversion rate
Stored in SMA coil spring	23.05 mJ	58.6%
Used for jumping	13.51 mJ	93.5%
Stored in sheet metal	12.63 mJ (Rotational spring: 11.84 mJ) (Axial spring: 0.79 mJ)	34.4%
Kinetic	4.34 mJ	91.6%
Potential	3.98 mJ	
The total conversion efficiency:		17.3%

sheet metal spring was deformed from 0 deg to 41.5 deg, and the stiffness was calculated as Eq. (2). Therefore, the stored elastic energy in each rotational spring was 5.92 mJ. In the case of the stamped axial sheet metal spring, it extended from initial neutral position, 15.7 mm, to maximum deflected position, 17.2 mm, and the stored energy in each axial spring was calculated as 0.4 mJ.

58.6% of the energy stored in SMA coil spring was used for jumping and 93.5% of used SMA elastic energy was transferred to the sheet metal springs. After snap-through, elastic energy was instantly released and converted to a translational kinetic energy of 4.34 mJ.

Finally, 34.4% of the energy stored in the elastic components was converted to translational kinetic energy. The loss occurs because of vibration and premature jumping. Therefore, the mechanical conversion efficiency of the jumping mechanism was given as 17.3%. Details are given in Table 3.

Conclusion

We proposed a novel fabrication method by using embedded sheet metal in the current method of layer-based manufacturing. The laminated sheet metal is partially bent for changing the neutral position by a stamping process, and the stamped sheet metal spring was simply modeled using PRBM. Based on the model, it is possible to design a sheet metal spring with the desired specifications. The designed sheet metal was applied to a small-scale bistable jumping mechanism, and the performance was demonstrated in jumping tests. The fabricated mechanism weighed only 2.3 g (including electronics), had a width of 5.1 mm, and a length of 22 mm. It is able to take off at a vertical speed of 1.93 m/s, contains 12.63 mJ of elastic energy, and can jump 175 mm in height.

In the future, the optimization between the rotational sheet metal spring and the stamped axial sheet metal springs is required to maximize the storable energy. Also self-righting mechanism should be developed for rejumping. Since the force–displacement relation of the stamped sheet metal varies depending on the radius and the angle of the die, more experiments are required while varying the die parameters. Furthermore, by increasing the number of nodes of stamped sheet metal, it is considered that a better performance may be obtained.

Acknowledgment

This research was supported by a grant to the Bio-Mimetic Robot Research Center, funded by the Defense Acquisition Program Administration under Grant No. UD130070ID. This work was also supported by Priority Research Centers Program through the National Research Foundation of Korea (NRF) funded by the Ministry of Education, Science and Technology (2014048162).

References

- [1] Scarfogliero, U., Stefanini, C., and Dario, P., 2006, "A Bioinspired Concept for High Efficiency Locomotion in Micro Robots: The Jumping Robot Grillo," IEEE International Conference on Robotics and Automation (ICRA 2006), Orlando, FL, May 15–19, pp. 4037–4042.
- [2] Kovac, M., Fuchs, M., Guignard, A., Zufferey, J.-C., and Floreano, D., 2008, "A Miniature 7 g Jumping Robot," IEEE International Conference on Robotics and Automation (ICRA 2008), Pasadena, CA, May 19–23, pp. 373–378.
- [3] Zhao, J., Xu, J., Gao, B., Xi, N., Cintrón, F. J., Mutka, M. W., and Xiao, L., 2013, "MSU Jumper: A Single-Motor-Actuated Miniature Steerable Jumping Robot," IEEE Trans. Rob., 29(3), pp. 602–614.
- [4] Lambrecht, B. G. A., Horchler, A. D., and Quinn, R. D., 2005, "A Small, Insect-Inspired Robot That Runs and Jumps," IEEE International Conference on Robotics and Automation (ICRA 2005), Apr. 18–22, pp. 1240–1245.
- [5] Fiorini, P., and Burdick, J., 2003, "The Development of Hopping Capabilities for Small Robots," Auton. Rob., 14(2–3), pp. 239–254.
- [6] Armour, R., Paskins, K., Bowyer, A., Vincent, J., and Megill, W., 2007, "Jumping Robots: A Biomimetic Solution to Locomotion Across Rough Terrain," Bioinspiration Biomimetics, 2(3), pp. S65–S82.
- [7] Matsuyama, Y., and Hirai, S., 2007, "Analysis of Circular Robot Jumping by Body Deformation," IEEE International Conference on Robotics and Automation, Rome, Italy, Apr. 10–14, pp. 1968–1973.
- [8] Gerratt, A. P., and Bergbreiter, S., 2013, "Incorporating Compliant Elastomers for Jumping Locomotion in Microrobots," Smart Mater. Struct., 22(1), p. 014010.
- [9] Noh, M. K., Kim, S. W., An, S. M., Koh, J.-S., and Cho, K. J., 2012, "Flea-Inspired Catapult Mechanism for Miniature Jumping Robots," IEEE Trans. Rob., 28(5), pp. 1007–1018.
- [10] Koh, J.-S., Jung, S.-P., Noh, M. K., Kim, S. W., and Cho, K. J., 2013, "Flea Inspired Catapult Mechanism With Active Energy Storage and Release for Small Scale Jumping Robot," IEEE International Conference on Robotics and Automation (ICRA), Karlsruhe, Germany, May 6–10, pp. 26–31.

- [11] Koh, J.-S., Jung, S.-P., Wood, R. J., and Cho, K. J., 2013, "A Jumping Robotic Insect Based on a Torque Reversal Catapult Mechanism," IEEE/RSJ International Conference on Intelligent Robots and Systems (IROS), Tokyo, Japan, Nov. 3–7, pp. 3796–3801.
- [12] Whitney, J., Sreetharan, P., Ma, K., and Wood, R. J., 2011, "Pop-Up Book MEMS," *J. Micromech. Microeng.*, **21**(11), p. 115021.
- [13] Lee, D.-Y., Koh, J.-S., Kim, J.-S., Kim, S.-W., and Cho, K. J., 2013, "Deformable-Wheel Robot Based on Soft Material," *Int. J. Prec. Eng. Manuf.*, **14**(5), pp. 1439–1445.
- [14] Wood, R. J., Avadhanula, S., Sahai, R., Steltz, E., and Fearing, R. S., 2008, "Microrobot Design Using Fiber Reinforced Composites," *ASME J. Mech. Des.*, **130**(5), p. 052304.
- [15] Hoover, A. M., Steltz, E., and Fearing, R. S., 2008, "RoACH: An Autonomous 2.4 g Crawling Hexapod Robot," IEEE/RSJ International Conference on Intelligent Robots and Systems (IROS 2008), Nice, France, Sept. 22–26, pp. 26–33.
- [16] Baisch, A. T., and Wood, R. J., 2011, "Design and Fabrication of the Harvard Ambulatory Micro-Robot," *Robotics Research*, C. Pradalier, R. Siegwart, G. Hirzinger, eds., Springer, Berlin, Germany, pp. 715–730.
- [17] Wood, R. J., Nagpal, R., and Wei, G.-Y., 2013, "Flight of the Robobees," *Sci. Am.*, **308**(3), pp. 60–65.
- [18] Koh, J.-S., and Cho, K. J., 2013, "Omega-Shaped Inchworm-Inspired Crawling Robot With Large-Index-and-Pitch (LIP) SMA Spring Actuators," *IEEE/ASME Trans. Mechatronics*, **18**(2), pp. 419–429.
- [19] Jung, G.-P., Koh, J.-S., and Cho, K. J., 2013, "Underactuated Adaptive Gripper Using Flexural Buckling," *IEEE Trans. Rob.*, **29**(6), pp. 1396–1407.
- [20] Howell, L. L., 2001, *Compliant Mechanisms*, Wiley, Hoboken, NJ.
- [21] Boljanovic, V., 2004, *Sheet Metal Forming Processes and Die Design*, Industrial Press Inc., Norwalk, CT.
- [22] Kazon, R., Firat, M., and Tiryaki, A. E., 2009, "Prediction of Spring Back in Wipe-Bending Process of Sheet Metal Using Neural Network," *Mater. Des.*, **30**(2), pp. 418–423.
- [23] Kim, S., Hawkes, E., Cho, K., Joldaz, M., Foley, J., and Wood, R., 2009, "Micro Artificial Muscle Fiber Using NiTi Spring for Soft Robotics," IEEE/RSJ International Conference on Intelligent Robots and Systems (IROS 2009), St. Louis, MO, Oct. 10–15, pp. 2228–2234.